
SEQUENTIAL IMAGE PROCESSING METHODS FOR IMPROVING SEMANTIC VIDEO SEGMENTATION ALGORITHMS

A PREPRINT

Beril Sirmacek, Nicolò Botteghi, Santiago Sanchez Escalonilla Plaza

Robotics and Mechatronics

University of Twente

Enschede, The Netherlands

(b.sirmacek, n.botteghi, s.sanchezescalonillaplaza)@utwente.nl

October 30, 2019

ABSTRACT

Recently, semantic video segmentation gained high attention especially for supporting autonomous driving systems. Deep learning methods made it possible to implement real-time segmentation and object identification algorithms on videos. However, most of the available approaches process each video frame independently disregarding their sequential relation in time. Therefore their results suddenly miss some of the object segments in some of the frames even if they were detected properly in the earlier frames. Herein we propose two sequential probabilistic video frame analysis approaches to improve the segmentation performance of the existing algorithms. Our experiments show that using the information of the past frames we increase the performance and consistency of the state of the art algorithms.

Keywords Artificial Intelligence · Semantic Segmentation · Conditional Probability · Temporal Consistency

1 Introduction

In an era for automation, it is not far fetched to think of a scenario where transportation does not suppose a hustle for the driver anymore. Regarding to commuting statistics, it is interesting to take a look at the American panorama as the living patterns are more standardized than over the different countries in Europe. A recent study by Statista [1] states that in America in 2016, an estimated 85.4 percent of 150M workers drove to their workplace in an automobile, while only 5.1 percent used public transportation for this purpose. Out of the 85.4 percent, a total of 77 percent (115M people) drove alone to work everyday [2].

Although some people enjoy the act of driving, it is fair to generalize that driving during rush hour is considered to be one of the most stressful scenarios for the daily commuting. While passengers can just sit and relax, the driver has to be constantly conscious about his actions during the whole ride. Self driving cars aim to free the driver from this activity, allowing him to spend his time in more valuable tasks. AC can also transform the current traffic system scenario by making it safer and more efficient to navigate, extending the benefits of automation to non-AC users.

Autonomous navigation however, is not a recent invention. In 1912, Lawrence Sperry successfully demonstrated the implementation of an autopilot-system on aviation. In an aircraft exhibition celebrated in Paris in 1914, Sperry performed numerous in-flight tricks in front of an audience to test the autonomy of the navigation system under no pilot conditions.

However, solving Autonomous navigation problems for cars, drones, bus, trucks... is not a trivial problem for different reasons:

- From the structural point of view, to list some examples: non-standardize roads (undefined or different lane sizes), inconsistent driving conditions (changes in weather, driving surface might deteriorate), obstacles or debris, ambiguous drivable space, undefined traffic signs location.

- From the non-structural point of view other factors come into play, such as: human or animal interaction (unpredictable behavior).

The eruption of deep learning on the last decade has allowed to create safer and more intelligent pilot systems that enable autonomous vehicles to operate better than under previously unseen scenarios. Deep learning together with the motivation of some companies to take autonomous navigation systems into mass production makes the present time to be the perfect one to solve the autonomous vehicles enigma.

1.1 Autonomous Navigation

Although any system that requires autonomous navigation (cars, drones or any other mobile robot) can be considered for this topic, this document will focus on autonomous cars. The reason for this focus is that the late outburst of autonomous navigation in the automobile industry is promoting the scientific interest towards autonomous cars resulting in new studies and data sets that cover this application.

When talking about autonomy, the National Highway Traffic Safety Administration (NHTSA) has defined the following levels of car automation:

- Level 0: No Automation. The driver performs all driving tasks.
- Level 1: Driver Assistance. The Vehicle is controlled by the driver, but some driving assists features may be included in the vehicle design (such as ESP, Airbags, Lane keeping,...)
- Level 2: Partial Automation. Driver-assist systems that control both steering and acceleration/deceleration, but the driver must remain engaged at all times (e.g. cruise control or parking assistance).
- Level 3: Conditional Automation. The driver is a necessity but not required at all times. He must be ready to take control of the vehicle at all times with notice.
- Level 4: High Automation. The vehicle is capable of performing all driving functions under certain conditions. The driver may have the option to control the vehicle.
- Level 5: Full Automation. The vehicle is capable of performing all driving functions under all conditions. The driver may have the option to control the vehicle.

There are different companies trying to adapt classic vehicles to the different levels of automation. Nowadays most of the cars available have at least a level 2 of automation making level 3 the next step of the challenge.

Level 3 is currently dominated by Tesla, since the release of autopilot in 2016, Tesla has been manufacturing new vehicles surpassing the 1 Billion miles mark driven autonomously (followed by Waymo with 10 Million miles). Despite this big improvement, further levels of automation require a deeper study of the current technology and gather big amounts of data from driving patterns and uncommon situations.

In order to grant cars with autonomy, former cars need to be upgraded both in the hardware as well as in the software side. A key piece for this upgrade is the choice of the car's equipment. Cameras are the most common sensor present in autonomous vehicles, which along with other type of sensors are able to recreate a virtual representation of the surroundings.

The application domain of autonomous driving extends to anyplace with a drivable area (figure 1). Apart from the variety of roads, the difficulty of automation is enhanced by the bounds of the problem: outdoors application. This loose definition of the domain specifications is what makes autonomous driving so challenging.



Figure 1: Different types of roads. From left to right: urban road, highway and rural road.

Granting a machine with the capacity of overtaking humans for tasks such as transportation is a non-trivial problem. Driving is a life-risk activity and therefore needs of a meticulous study, testing and evaluation of these new autonomous technologies.

1.2 Semantic image segmentation

Computer Vision is the field of engineering that focuses on the extraction of the information encoded on images for its use on different applications. Classical computer vision extracts this information through the calculation of different image descriptors. The calculation of the image descriptors is conditioned by the system characteristics: image resolution, object shape, light conditions, application domain. The process that defines the image descriptors derivation is called feature extraction.

Image descriptors are usually designed as hand-engineered filters, providing solutions that are rather rigid (application specific) and reliable only under very restricted conditions. Unfortunately autonomous navigation falls into a completely opposite scenario, requiring of applications that can perform robustly under very dynamic circumstances.

The main advantage of deep learning is its flexibility to generalize to previously unseen data. Since the application of Convolutional Neural Networks (CNNs) [3] for image processing, Deep Learning has been the protagonist on countless Computer Vision conferences and research papers. CNNs allow the extraction of features in a more efficient and meaningful way than classical image descriptors, based on image gradient calculations. Standing out due to their capacity of automation of image descriptors, CNNs allow the creation of Image Processing applications with a high level of abstraction and accuracy.

Semantic image segmentation (figure 2) is just one of the many Deep Neural Networks (DNN) applications. The goal Semantic Segmentation application is to detect and classify objects in the image frame by applying pixel-level classification of an input image into a set of predefined categories. Semantic image segmentation provides a level of scene understanding much richer than any other detection algorithms, it includes detailed information about the shape of the object and its orientation. Semantic segmentation can be used in autonomous navigation to precisely define the road (or drivable space) and its conditions (erosion, presence of obstacles or debris), it is also very useful for navigation in crowded areas being able to accurately calculate the gap between obstacles and even make predictions of the future position of the obstacles based on its shape and trajectory. Semantic image segmentation models can generally be divided into two parts: the feature extraction layers (hidden layers) and the output layers. The feature extraction layers use CNNs along with other techniques such as pooling or skip connections to obtain a low level representation of the image. And the output layers create the necessary relations to draw-out the pixel classification.

The scope of the project will be restricted to the analysis of a hypothetical video feed coming from the frontal camera of an autonomous car. The purpose of this camera is to elaborate a frontal representation of the environment that can be used for navigation. Flying objects, dirt or sun glare are some of the external factors that can affect the correct performance of cameras. In order to guarantee the passengers' safety, the detection system of autonomous cars must stand out for the robustness and consistency of its results and all these situations need to be considered. An additional observation is that when applied to autonomous navigation applications, the segmentation should prevail the detection of obstacles over driving space to ensures the avoidance collisions.



Figure 2: Ideal result of a semantic image segmentation. In this figure, all the objects that conform the image are perfectly classified into the different colors that define each category: road, sidewalk, pedestrian, tree, building or traffic sign. This image is part of the Cityscapes groundtruth densely annotated dataset. Cityscapes is a large-scale data set created as tool to evaluate the performance of vision algorithms intended for semantic urban scene understanding and help researchers to exploit large volumes of annotated data. Image source: [4].

2 Problem statement

Semantic segmentation allows autonomous cars to obtain an accurate representation of the outside world. This representation is used to define the available navigation space and the presence of obstacles necessary to calculate navigation trajectories.

Figure 2 shows an example of a perfect semantic image segmentation, however it is very difficult to obtain a segmentation in such a high level of detail. The deep learning model would require large amounts of high resolution finely annotated and varied data to allow the training optimization algorithm reach the desired accuracy while not overfitting. In contrast, figure 3 shows a real example of how an image that has been processed using an out-of-the-box state-of-the-art semantic image segmentation model (DeepLabv3 [5]) that was trained on the Cityscapes data set [6] looks like. Figure 3

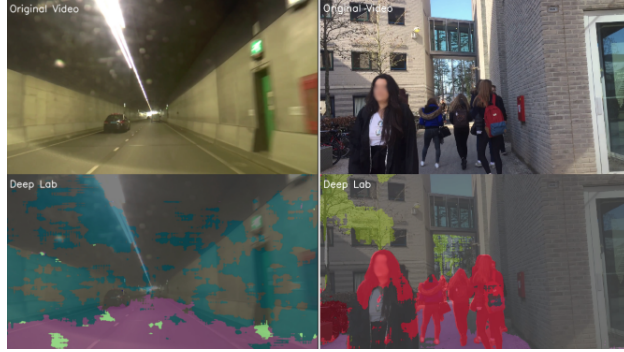


Figure 3: Figure illustration of the segmentation level obtained by DeepLabv3 [5], the current state-of-the-art semantic image segmentation model trained on the Cityscapes dataset [6]. This figure illustrates two different levels of segmentation imperfection. Left image: example of a totally missed classification of the cars in front of the camera, added to a noisy classification of the road and the walls. Right image: example of a partial segmentation of the pedestrians.

illustrates how the current level of a semantic image segmentation state-of-the-art model performance differs from the ground-truth example shown on figure 2. Although a partial classification might be good enough for obstacle avoidance, in some cases the semantic image segmentation model completely misses the classification of the obstacle and therefore can cause an accident. For this reason, autonomous cars have numerous sensors that allow the detection of obstacles at different distance ranges not relying on bare-semantic image segmentation models as the main source of information.

Another of the effects that can be observed after applying semantic image segmentation models for the analysis of videos is temporal inconsistency. Analyzing a video frame by frame causes a segmentation that is not consistent over time, small variations in the frame produce high variances in the segmentation .

This study examines *how to reduce the incorrect classifications produced by semantic image segmentation models by combining the information of neighbouring frames* In an attempt to improve the obstacle detection, this study can be broken down into the following research questions:

- *Analysis of the state-of-the-art: what is the current state-of-the-art for semantic image segmentation?*
- *Temporal extension: how to extend semantic-image-segmentation models for the analysis of sequences?*
- *Reducing missed classifications: what kind of mechanisms can be applied to reduce the number of false classifications?*

3 Background

As previously stated, one of the main goals of this article is *how to extend semantic image segmentation models for the analysis of sequences* (videos are a sequence of images). The main difference between images and videos is that the latter consists of a group of images (frames) that are adjacent in time, indirectly encoding a temporal history. In order to exploit the sequential information present in videos, this section will introduce the available tools capable of modeling sequences. In section 5, some of these techniques will be used with a semantic image segmentation model in an attempt to add the video temporal information into the segmentation.

Given a causal system, sequence modeling consists on elaborating a model that is able to reproduce the dynamic behavior present in the observed data. From probabilistic methods to neural networks, this section summarizes different procedures used to capture temporal dynamics.

The methods reviewed in this section can be divided into two different groups depending on the tools used for sequence modeling: Conditional Probability and Deep Learning Architectures. The first one reviews causal modeling using probability relations. The second one introduces deep neural networks that have been specifically designed for modeling videos.

3.1 Sequence Modeling: Conditional probability

This section analyzes how to model the association between variables using probabilistic relations. Given two observed variables ' x_1 ' and ' x_2 ', the conditional probability of ' x_2 ' taking a value given that ' x_1 ' takes another value (two different events) is defined as [7]:

$$P(x_2|x_1) = \frac{P(x_1, x_2)}{P(x_1)}, \text{ if } P(x_1) > 0 \quad (1)$$

Where the numerator of equation 1 is the joint probability of both events happening at the same time, and the denominator is the marginal probability of event ' x_1 '. It is possible to extend this notation to cover a bigger set of events (or a sequence of events). For a set of variables $X_t = x_1, x_2, \dots, x_t$ (for $t > 0$), the probability of the variable x_t conditioned to the rest of the variables in ' X_t ' is:

$$P(x_t|\{X_\tau, \tau \neq t\}) = \frac{P(x_1, x_t)}{P(x_1, \dots, x_{(t-1)})} = \frac{P(X_t)}{P(\{X_\tau, \tau \neq t\})}, \text{ if } P(\{X_\tau, \tau \neq t\}) > 0 \quad (2)$$

Besides expressing the relation between variables using conditional probability notation, it is also possible to use graphical models or probabilistic graphical models. A Probabilistic Graphical Model (PGM) is a graph that expresses the conditional dependence relation between random variables. Conditional probability notation in combination with probabilistic graphical models are commonly used in fields such as probability theory, statistics and machine learning.

A possible graphical representation of equation 2 for $t = 4$ can be found in figure 4 There are two main approaches that

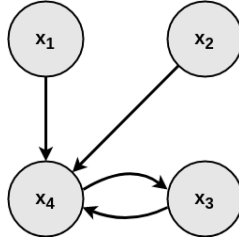


Figure 4: Possible probabilistic graphical model of equation 2 for $t = 4$. In this graph, ' x_4 ' depends on ' x_1, x_2 and x_3 '; ' x_3 ' depends on ' x_4 '; and ' x_1 and x_2 ' are independent.

can be followed when defining the probability model for a dynamic system: a generative approach or a discriminative approach. Although the final purpose of both approaches is the same, to sample data from a probability distribution, each approach is different.

Generative models focus on modeling how the data is generated, in other words, modelling the joint probability $P(X_t)$, where ' X_t ' is the set of variables involved in the process— e.g. in retrospect to the analysis of videos, each variable in ' X_t ' can represent the value of a pixel over consecutive time steps, and ' t ' the frame index. A generative model is able to calculate the joint distribution of all the present variables ' $P(X_t)$ '. For the simple case of having 4 variables, modeling ' $P(X_4)$ ' allows finding all the possible combinations for these variables: having observed the pixel at times 1, 2 and 3, it is possible to estimate x_4 ; or any other combination, such as computing x_2 given x_1, x_3 and x_4 .

On the other hand discriminative models only focus on modeling the conditional relation between variables (equation 2), not paying attention on how the data is generated— e.g. having observed x_1, x_2 and x_3 it is possible to estimate x_4 but it does not allow to compute any other combination for the variables.

From the definition, generative models may appear to be more general and insightful about the present dynamic system than the discriminative ones. However, discriminative models are often preferred for classification tasks such as logistic regression [8]. The reason for this preference is that the generalization performance of generative models is often found to be poorer than the one proper of discriminative models due to differences between the model and the true distribution of data [9].

The most common procedures to create probability models will be reviewed in the following order: Naive Bayes Classifiers, Markov Chains and Hidden Markov Models (HMM).

3.1.1 Naive Bayes Classifier

The Naive Bayes classifier is a generative approach because it models the joint probability ' $P(X_t)$ ' and afterwards calculates the conditional probability applying the Bayes Rule. Starting from the definition of conditional probability

(equation 2), it is possible to apply the product rule of probability to the numerator, ' $P(X_t)$ ' as:

$$P(X_t) = P(\{X_\tau, \tau \neq t\}, x_t) = P(\{X_\tau, \tau \neq t\}|x_t) \cdot P(x_t) \quad (3)$$

And the sum rule to the denominator to define $P(X_{(t-1)})$ as the marginal distribution of $P(X_t)$:

$$P(\{X_\tau, \tau \neq t\}) = \sum_T P(\{X_\tau, \tau \neq t\}, x_t) = \sum_T P(\{X_\tau, \tau \neq t\}|x_t = T) \cdot P(x_t = T) \quad (4)$$

where T comprehends all the possible states of x_t .

The Bayes Rule is the result of applying these two properties to the definition of conditional probability (equation 2):

$$P(x_t|\{X_\tau, \tau \neq t\}) = \frac{P(X_t)}{P(\{X_\tau, \tau \neq t\})} = \frac{P(x_t) \cdot P(\{X_\tau, \tau \neq t\}|x_t)}{\sum_T P(x_t = T) \cdot P(\{X_\tau, \tau \neq t\}|x_t = T)} \quad (5)$$

The general form of the Bayes Theorem says that *the posterior probability of an event is proportional to the prior probability of that event times the likelihood of the observation conditioned to that event*. In other words, if the probability of a given variable (or set of variables) $P(\{X_\tau, \tau \neq t\})$ is fixed, the posterior probability (equation 5) can be expressed as a proportional factor of the numerator.

Using the previous example that tracks the value of a pixel over 3 consecutive frames, the value of the pixel at time frame 4 will be given by:

$$P(x_4|X_3) \propto P(x_4) \cdot P(X_3|x_4) \quad (6)$$

In a more general form, the conditional probability of a state x_t given a set of previous observations from x_1 to $x_{(t-1)}$:

$$P(x_t|\{X_\tau, \tau \neq t\}) \propto P(x_t) \cdot P(\{X_\tau, \tau \neq t\}|x_t) \quad (7)$$

The Naive Bayes assumption states that the features (observations $X_{(t-1)}$) are conditionally independent given the class label (x_t)[7].

Applying the Naive Bayes assumption of independence allows to exploit the second term of equation 7 into ' $t - 1$ ' different terms:

$$P(\{X_\tau, \tau \neq t\}|x_t) = P(x_1|x_t) \cdot P(x_2|x_t), \dots, P(x_{(t-1)}|x_t) P(x_t|\{X_\tau, \tau \neq t\}) \propto P(x_t) \prod_{n=1}^{(t-1)} P(x_n|x_t) \quad (8)$$

Equation 8 defines a model that predicts the value for the state x_t for a set of observed states $X_{(t-1)} = (x_1, x_2, \dots, x_{(t-1)})$. It is the final form of the Naive Bayes classifier, which as a consequence of the Naive Bayes assumption do not capture dependencies between each of the observed states in $X_{(t-1)}$ (figure 5). Even though this conditional independence assumption might sound unrealistic for real case scenarios, empirical results have shown a good performance in multiple domains with attribute dependencies [10]. These positive findings can be explained due to the loose relation between classification and probability estimation: 'correct classification can be achieved even when the probability estimates used contain large errors' [10].

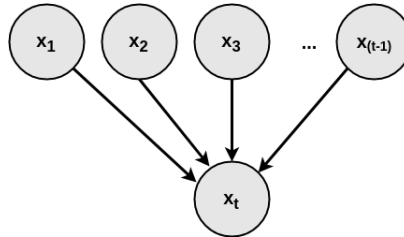


Figure 5: Graphical representation of the final form Naive Bayes classifier. It is based on the Naive Bayes assumption that states that: the observations $(x_1, \dots, x_{(t-1)})$ are conditionally independent given the value of x_t .

Markov Models and Hidden Markov Models do not make any assumptions about the in-dependency of the variables and will be illustrated next.

3.1.2 Markov Chains

Markov chains or Markov Models (MM) are stochastic generative models for dynamic systems that follow the Markov property. Markov's property states that the future state of a variable depends only on the current observation (there is only dependence between adjacent periods). In the framework of video processing, Markov's property can be interpreted as: the value of a pixel in the present is only dependent on its immediate past (figure 6).

Using probabilistic notation, Markov's property can be applied as:

$$P(x_t|\{X_\tau, \tau \neq t\}) = P(x_t|x_{t-1}) \quad (9)$$

Where $\{X_\tau, \tau \neq t\}$ contains all the previous states from x_1 to x_{t-1} . The resulting joint probability of a Markov chain like the one present in figure 6, is defined as:

$$P(X_t) = P(x_1)P(x_2|x_1)P(x_3|x_2)\dots = p(x_1) \prod_{t=2}^T P(x_t|x_{t-1}) \quad (10)$$

In discrete-MM, the variables can only take certain values from a set of possible states that differ from each other. For a set of N possible states, there is a N by N transition matrix that contains the probabilities of transitioning between states. Figure 6 shows an example of a MM with two possible states x_1 and x_2 , the transition probabilities that define this MM can be found in table 1.

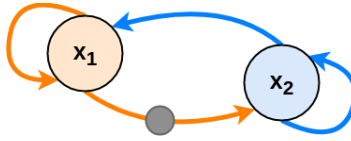


Figure 6: Graphical representation of a Markov Model with two possible states: x_1 and x_2 . The connections between states represent the possible paths that the current state can follow. The values that condition each path are usually contained in a transition table (table 1). The dark circle is current state transitioning from x_1 to x_2 . Image adaptation from: [11].

	x_1	x_2
x_1	$P(x_1 x_1)$	$P(x_2 x_1)$
x_2	$P(x_1 x_2)$	$P(x_2 x_2)$

Table 1: Transition matrix of a Markov Model with two possible states (x_1 and x_2).

In a discrete stochastic process, the rows of a transition probability matrix have to sum up to one, which means that a state has a finite amount of possible states. The values inside the transition matrix can be: given; calculated gathering samples from the process, doing a statistical analysis of the data and assuming that the process follows a certain distribution; or approximated using probability distribution approximation methods such as the Metropolis-Hastings algorithm, that assumes an initial probability distribution and through several iterations it moves it closer to the real distribution [7].

The strong assumption made in equation 9 can be relaxed by adding dependence with more than one past states, transforming the MM into a k-order Markov chain. A second order Markov chain is illustrated in figure 7.

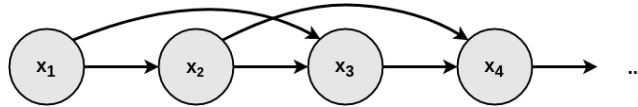


Figure 7: Graphical representation of a second order Markov chain. Image adaptation from: [7]

The corresponding joint probability of a second-order Markov chain follows the next equation:

$$P(X_t) = P(x_1, x_2)P(x_3|x_1, x_2)P(x_4|x_2, x_3)\dots = p(x_1, x_2) \prod_{t=3}^T P(x_t|x_{t-1}, x_{t-2}) \quad (11)$$

Equations 9 and 11 can be applied where the for processes where the state of the system can be directly observed. However, in many applications, the state is not directly observable, these are called Hidden Markov Models and will be defined next.

3.1.3 Hidden Markov Model

Hidden Markov models (HMM) also belong to the stochastic generative models category. They differ from Markov chains because the state variables ' $Z_t = (z_1, z_2, \dots, z_t)$ ' are not anymore directly accessible, i.e. hidden variables, and only the variables ' $X_t = (x_1, x_2, \dots, x_t)$ ' are observable.

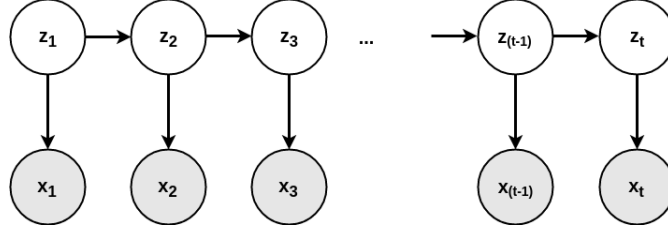


Figure 8: Graphical representation of a first order hidden Markov model. Image adaptation from: [7]

Figure 8 shows the representation of a first order HMM. There are two equations necessary to define this HMM. The relation between observable variables X_t and hidden processes Z_t ; and the relation between hidden processes with each other:

$$P(x_t|\{X_\tau, \tau \neq t\}, Z_t) = P(x_t|z_t)P(z_t|\{Z_\tau, \tau \neq t\}) = P(z_t|z_{(t-1)}) \tag{12}$$

Resulting in the following joint distribution:

$$P(Z_t, X_t|Z_i) = P(X_t|Z_t)P(Z_t|\{Z_\tau, t-1 \leq \tau < t\}) = P(z_1, x_1|z_1) \prod_{t=2}^T P(x_t|z_t)P(z_t|z_{(t-1)}) \tag{13}$$

The probabilities that relate hidden states ' z_t ' (equation 12) are called transition probabilities, while the probabilities that associate hidden processes with observable variables ' x_t ' (equation 12) are the emission probabilities. Both of them can be calculated in an analogous way to the transition probabilities for the Markov chains (table 1).

Markov Models and Hidden Markov Models, although more general than the Naive Bayes Classifier, are also limited by definition. Each state is defined only to be affected by a finite number of previous states ' k ' and the effect of any other states happening before ' $t - k$ ' is assumed to be encoded in this period, this limitation is often described as a short-term memory problem. Trying to find patterns in the sequence to determine the k-gram dependencies beforehand can help to alleviate this issue [12].

This section has introduced different methods that are used to model sequential information from the probabilistic theory point of view. Next section introduces different approaches used to overcome temporal context using deep learning architectures.

3.2 Video Modeling: Deep Learning Architectures

Considering videos as sequences of static images, this section can serve as an introduction to different approaches used to add temporal context to the analysis of videos.

3.2.1 Gated Recurrent Flow Propagation - GRFP

Seeking to solve the semantic segmentation inconsistency characteristic of evaluating video segmentation with individual image segmentation methods, [13] announced a method that combines nearby frames and gated operations for the estimation of a more precise present time segmentation.

The Spatio-Temporal Transformer GRU (STGRU) in [13], is a network architecture that adopts multi-purpose learning methods with the final purpose of video segmentation. Figure (9) shows a scheme of the STGRU architecture. Inside of the STGRU, FlowNet is in charge of calculating the optical flow for N consecutive frames. A wrapping function (ϕ) uses this optical flow to create a prediction of the posterior frame. Later, a GRU compares the discrepancies between the estimated frame (w_t) and the current frame evaluated by a baseline semantic segmentation model (x_t), keeping the areas with higher confidence while resetting the rest of the image.

The STGRU presented in [13] was evaluated both quantitatively and qualitatively (fig. 10), exhibiting a high performance compared with other segmentation methods.

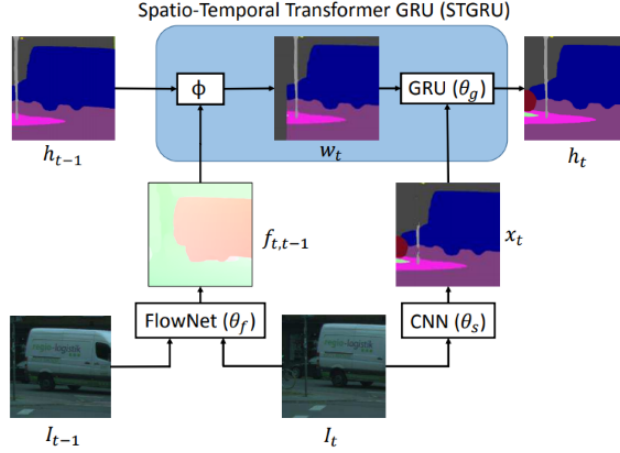


Figure 9: Overview of the Spatio-Temporal Transformer Gated Recurrent Unit. Pairs of raw input images are used to calculate the optical flow of the image (FlowNet). This optical flow is then combined with the semantic segmentation of the previous frame, obtaining a prediction of the present segmentation (blue box). A segmentation map of the present frame is then passed together with the prediction to a GRU unit that combines them based on the sequence. Image source: [13]

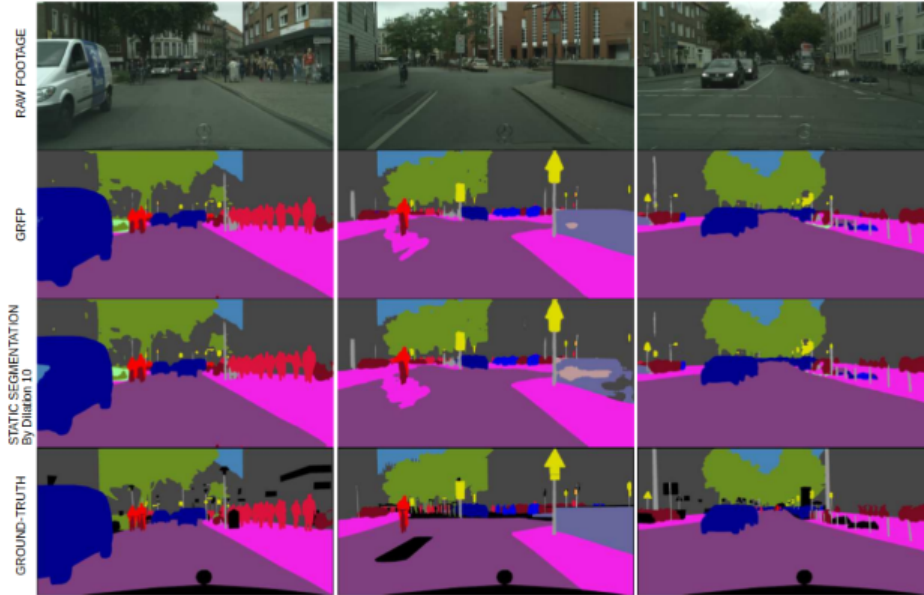


Figure 10: Image adaptation from Nelsson et al. [13]. In this image it can be seen a comparison between: GRFP method, Static Semantic Segmentation and the groundtruth segmentation. From left to right, GRFP achieves a segmentation improvement for the left-car, the right-wall and the left-pole.

3.2.2 Other architectures for video applications

The current trend for semantic video segmentation models consists on combining multipurpose neural networks (sequence modelling with feature extraction networks) into advanced models capable of efficiently performing this task. Some other video segmentation architectures include:

- Feature Space Optimization for Semantic Video Segmentation [14].
- Multiclass semantic video segmentation with object-level active inference [15].
- Efficient temporal consistency for streaming video scene analysis [16].

Semantic image segmentation is not the only application in computer vision that can benefit from leveraging temporal context, tracking also use temporal analysis tools to achieve a better performance. The main reasons why temporal context is necessary for tracking are to guarantee the detection of the object even through occlusion and to reduce the number of identity switches (during multiple object tracking). These kind of applications are very common on surveillance or sport events. In 2017, [17] combined image appearance information with other tracking methods (Simple Online Real-time Tracker [18]) based on Kalman Filter and the Hungarian algorithm to obtain state-of-the-art detection at high rates (40Hz).

4 Analysis

This section provides a detailed description of the problem and the materials that will be used for the study.

4.1 Domain Analysis

4.1.1 Semantic segmentation for Autonomous cars

Semantic segmentation is considered one of the hardest computer vision applications. It differs from image classification or object detection in how the classification is performed (figure 11). Image classification models classify the image globally, they assign a label to the whole image (e.g. cat or dog image classifier). Object detection models look for patterns in the image and assign a bounding box to the region of the image that is more likely to match with the target description (it provides classification and location within the image). And semantic segmentation produces pixel-level classification of an image; it describes each pixel of the image semantically, providing a more insightful description of how the image is composed than the other two methods.

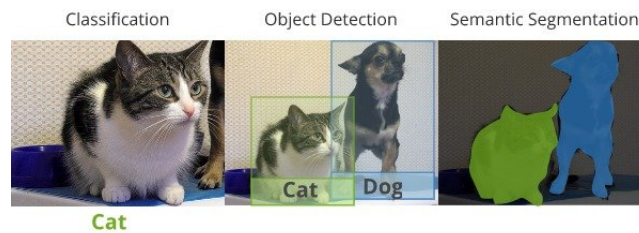


Figure 11: Figure comparison of the three computer vision classification applications. From left to right: image classification (global classification), object detection (local classification) and semantic segmentation (pixel-level classification). Image source: [19]

Humans are very good at segmentation of images, even without knowing what the objects are. This is the main reason why semantic image segmentation is necessary for autonomous navigation. Although other detection models are able to classify obstacles and locate them in the space, they can only find the obstacles they have previously seen. E.g. an obstacle detector used to avoid pedestrians in autonomous cars, it will only be able to alert the vehicle in the presence of pedestrians (it was just trained to learn how the pedestrian category is modeled). However, the type of obstacles that can be found in a undefinable driving scenario (it covers any object in any kind of shape and it is not feasible to create a data set that covers for all), this is the reason why semantic image segmentation is present in autonomous navigation. An ideal semantic image segmentation model will be able to define the boundaries of any objects, even when these objects have not been previously 'seen' (figure 12). Apart from being a good obstacle detector, a perfect semantic image segmentation model has the ability to store these previously unseen objects, tag them and use them to re-train the network and improve the accuracy.

There are some requirements that need to be present when applying semantic segmentation into autonomous navigation. The vehicle receives the data as a stream of images (it does not count with a video of the route beforehand) and it has to perform inference in real-time. The model should be very sensible on the detection of obstacles, e.g in an ambiguous situation where the segmentation of the road is not perfectly clear, due to imperfections or the presence of objects, the classification of obstacles must prevail.

4.1.2 Software analysis

The most common programming languages used for computer vision and deep learning applications are Python and C++. The former is preferred on the research scope, while the latter is mainly used in commercial applications. Apart



Figure 12: Adverse situations that can be solved using semantic image segmentation. Object detection models can only to detect objects that the model is familiar with. However, it is very difficult to create a dataset that includes all the possible types of obstacles, imperfections or debris that may appear in the road. Semantic image segmentation aims to achieve perfect definition of the image even when the objects are unknown.

from the programming languages, there are different frameworks that provide the developer with the tools required to handle big amounts of data: Theano, PyTorch, TensorFlow or Keras are some of the frameworks compatible with both Python or C++.

Although the programming language and deep learning framework affect the performance of the application, the final performance only depends on the implementation algorithm (semantic image segmentation model). As a matter of preference, this study is developed using Python and Tensorflow.

4.1.3 Semantic image segmentation model selection

Depending on its inner structure, the different semantic image segmentation models are able to obtain different levels of segmentation accuracy and inference speed. Figure 13, although it is not up to date, shows some of the available possibilities arranged by accuracy and inference speed on Cityscapes dataset [6]. Cityscapes is a large-scale urban-scene dataset that contains high resolution fully annotated segmentation images for semantic segmentation applications (section 4.1.5).

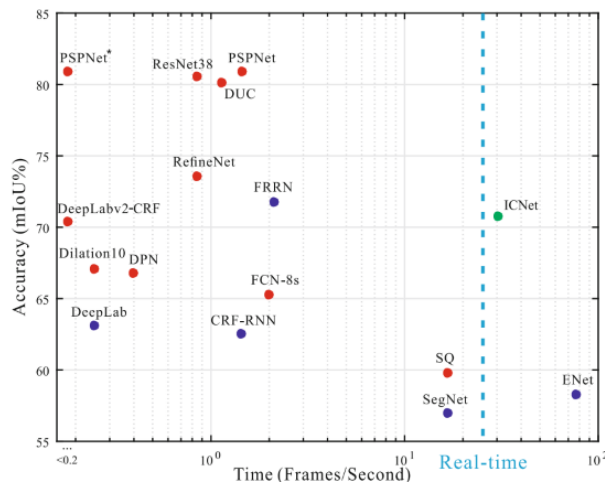


Figure 13: Classification of different semantic image segmentation models according to inference speed and accuracy (mIoU) on Cityscapes test set [6]. It can be observed how faster models (bottom-right corner) usually achieve a lower level of accuracy than slower ones (upper-left corner). Image source: [20].

In figure 13, the inference speed was measured by counting the amount of frames that the segmentation model is able to process each second. The mIoU (mean Intersection over Union) measures the mean accuracy of all the frames processed at each speed. As a result, the upper-left corner contains the most accurate (but slower, $\sim 0 - 1$ frames per second) models while the less accurate (but faster, $\sim 10 - 100$ frames per second) are grouped on the bottom-right corner.

Later in the same year of the release of the study in figure 13, Chen et al. [5] in their paper *Rethinking Atrous Convolution for Semantic Image Segmentation*, introduced DeepLabv3, a new iteration of the DeepLab model series that became the state-of-the-art for semantic image segmentation models on Cityscapes test set (table 2).

In order to continue with state-of-the-art efficiency, DeepLabv3 [5] with pretrained-weights on Cityscapes dataset [6] is chosen as the baseline model for this study.

Method	mIOU
DeepLabv2-CRF [21]	70.4
Deep Layer Cascade [22]	71.1
ML-CRNN [23]	71.2
Adelaide_context [24]	71.6
FRRN [25]	71.8
LRR-4x [26]	71.8
RefineNet [27]	73.6
FoveaNet [28]	74.1
Ladder DenseNet [29]	74.3
PEARL [30]	75.4
Global-Local-Refinement [31]	77.3
SAC_multiple [32]	78.1
SegModel [33]	79.2
TuSimple_Coarse [34]	80.1
Netwarp [35]	80.5
ResNet-38 [36]	80.6
PSPNet [37]	81.2
DeepLabv3 [5]	81.3

Table 2: Table comparison of the performance of different semantic image segmentation models on the Cityscapes dataset [6]. Table adaptation: [5].

4.1.4 DeepLabv3

DeepLabv3 [5], developed by Google, is the latest iteration of the DeepLab model series for semantic image segmentation— previous versions: DeepLabv1 [38] and DeepLabv2 [21].

DeepLab is based on a fully convolutional layer architecture (FCN) that employs atrous convolution with upsampled filters to extract dense feature maps and capture long range context [5]. [39] showed how powerful convolutional networks are at elaborating feature models and defined a FCN architecture that achieved state-of-the-art performance for semantic segmentation on the PASCAL VOC benchmark [40]. Another of the advantages of using FCN is that the architecture is independent of the input size, they can take input of arbitrary size and produce correspondingly-sized output [39]. In contrast, architectures that combine Convolutional Networks (for feature extraction) with Fully-Connected Conditional Random Fields (for classification)[21, 38] are designed for a fixed input size, as a result of the particular size necessary to pass through these classification layers.

One main limitation of solving semantic segmentation using Deep Convolutional Neural Networks (DCNNs) are the consecutive pooling operations or convolution striding that are often applied into the DCNNs, consequently reducing the size of the feature map. These operations are necessary in order to increasingly learn new feature abstractions [41], but may impede dense prediction tasks, where detailed spatial information is desired. Chen et al. [5] suggest the use of 'atrous convolution' as a substitute of the operations that reduce the size of the input (figure 14).

Atrous convolution, is also known as a dilated convolution. Apart from the kernel size, dilated convolutions are specified by the dilation rate, that establishes the gap between each of the kernel weights. A dilation rate equal to one corresponds to a standard convolution, while a dilation rate equal to two means that the filter takes every second element (leaving a gap of size 1), and so on (figure 15). The gaps between the values of the filter weights are filled by zeros, the term 'trous' means holes in French. [21, 38, 42] show how effective the application of dilated convolution is in maintaining the context of the features.

A second limitation faced by semantic image segmentation models is that they have to detect objects at multiple scales. This is a problem when using regular sized filters (normally 3x3) because they can only 'see' in regions of 9 pixels at a time, which makes it very difficult to capture the overall context of big objects. DeepLabv3 [5] employs Atrous Spatial Pyramid Pooling (ASPP) to overcome this issue, it consists on applying atrous convolution with different dilation rates over the same feature map and concatenate the results before passing it into the next layer figure 16. This approach helps capturing feature context at different ranges without the necessity of adding more parameters into the architecture (larger filters) [21, 43, 44]. Figure 17 shows the final architecture of DeepLabv3. Blocks 1 to 3 contain a copy of the original last block in ResNet [5]; which consists of six layers with 256 3x3 kernel convolution filters (stride=2), batch

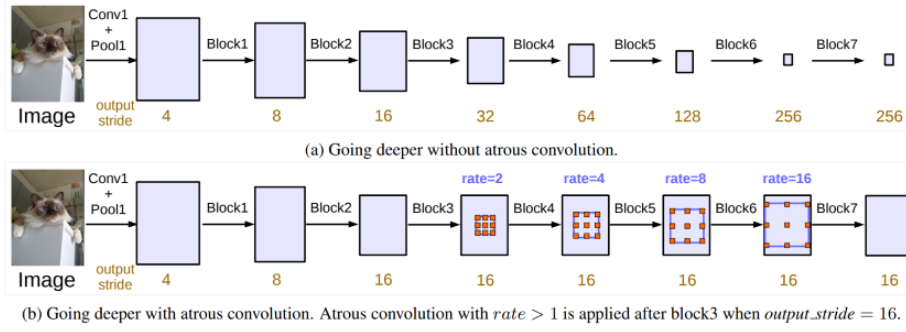


Figure 14: This figure compares the effect of consecutive pooling or striding to the feature map. (a) Shows an example where the feature map in the last layers is condensed to a size 256 times smaller than the input image, this is harmful for semantic segmentation since detail information is decimated [5]. (b) Applies atrous convolution to preserve the output stride obtaining equivalent levels of abstraction [5]. Image source: [5]

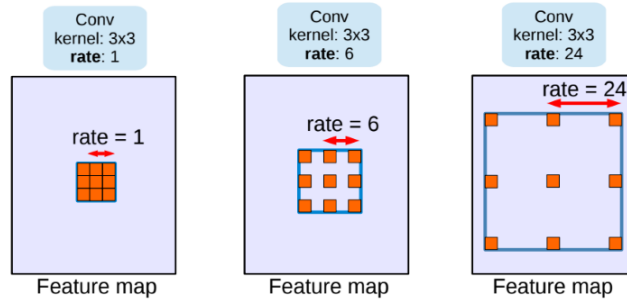


Figure 15: Atrous convolution of a filter with kernel size 3x3 at different stride rates. The dilation rate determines the space in between the different cells of the kernel. A rate=1 corresponds to the standard convolution, a rate=6 means that weights of the kernel are applied every sixth element (gap of 5 units), and so on. Image source: [5].

normalization right after each convolution and skip connections every 2 layers [46]. Block 4 is equivalent to the first 3 but it applies atrous convolution with dilation rate of 2 as a substitute of downsampling the image with convolutions of stride 2, maintaining the output stride to 16. The next block applies ASPP at different rates and global average pooling of the last feature map, all the results of this block are then concatenated and passed forward. The resulting features from all the branches are then concatenated and passed through a 1x1 convolution before the final 1x1 convolution that generates the final logits [5]. The output image consists on a $H \times W \times C$ matrix where H and W correspond to the height and width of the output image and C is the number of categories in the dataset. Every pixel is assigned a real number for each category, that represents the likelihood (or logits) of that pixel belonging to each category, this is called the score map. The score map is then reduced by means of an argmax operation that determines the index of the category with the highest likelihood, obtaining the semantic segmentation map.

4.1.5 Cityscapes dataset

Cityscapes is the state-of-the-art dataset for urban scene understanding. It was created out of the lack of available datasets that adequately captured the complexity of real-world urban scenes. Despite the existence of generic datasets for visual scene understanding such as PASCAL VOC [40], the authors of Cityscapes claim that "*serious progress in urban scene understanding may not be achievable through such generic datasets*" [6], referring to the difficulty of creating a dataset that can cover any type of applications.

Nonetheless, Cityscapes is not the only dataset of its kind. Other datasets such as CamVid [47], DUS [48] or KITTI [49] also gather semantic pixel-wise annotations for the application in autonomous driving. Cityscapes is the largest and most diverse dataset of street scenes to date [6], it counts with 25000 images (figure 18) from which 5000 are densely annotated (pixel-level annotation) while the remaining 20000 are coarsely annotated (using bounding polygons, which offers a lower level of detail). Compared to the other datasets purposed for autonomous driving, Cityscapes has the largest range of traffic participants (up to 90 different labels may appear in the same frame)[6] and has the largest range for object distances, covering objects up to 249 meters away from the camera [6].

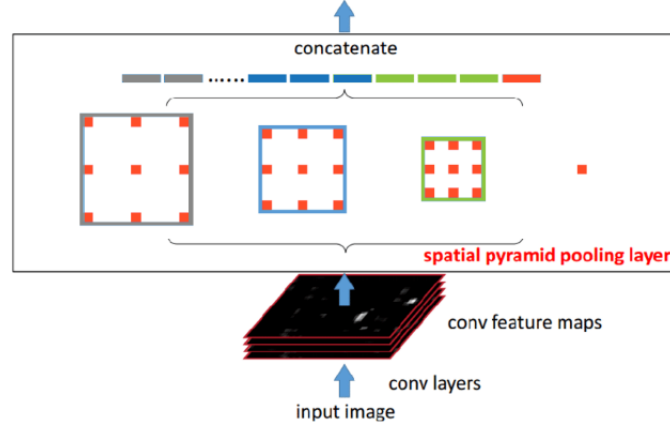


Figure 16: Graphical representation of ASPP. Atrous convolution with different dilation rates is applied on the same feature map, the result of each convolution is then concatenated and passed to the next layer. Spatial pyramid pooling is able to capture feature context at different ranges[21, 43, 44]. Image adaptation: [45]

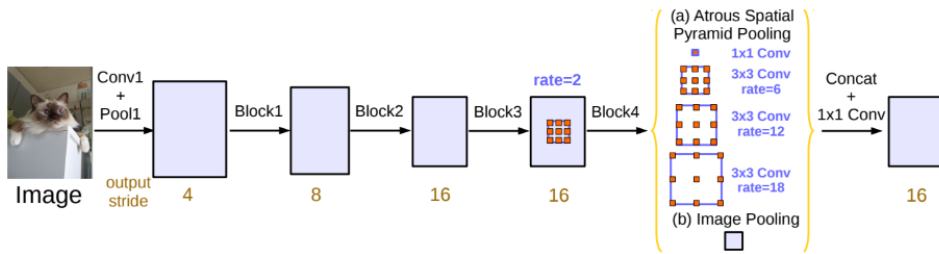


Figure 17: DeepLabv3 architecture. The first 3 blocks are a replica of the last block of the original residual neural network [46]. The following blocks incorporate the use of atrous convolution and ASPP, which stops the output stride reduction to 16, diminishing the negative effects of consecutive pooling. Image source: [5]

All these characteristics make the Cityscapes dataset the most challenging urban-scene understanding benchmark to date, "algorithms need to take a larger range of scales and object sizes into account to score well in our benchmark"[6]. Yet there are some limitations that need to be considered when evaluating the performance of a model that has been trained using this dataset. Cityscapes only captures urban areas (inner-city) of cities primarily from Germany or neighbouring countries [6], which may turn in a low efficiency when applied to highways, rural areas or other countries (due to differences in the architectures). The original images were taken during spring and summer seasons and do not cover situations with adverse weather conditions and or poor illumination. More information about the composition and a statistical analysis of this dataset can be found in [6].

4.2 Methodology

After several test runs of the baseline model on image sequences, it was observed that the production of wrong classifications (completely or partially missed object's classification) is a transitory effect. When applied on a sequence of images, the baseline model is usually able to detect most of the objects producing segmentation of different qualities on each frame. Differences in the lighting conditions or noise in the image may be the cause of this variation from frame to frame. However, **this is an effect that can be exploited in order to achieve a better segmentation.**

The next conclusion came after analyzing a moving object over consecutive frames. The moving object was recorded using a regular camera (at 30fps), it was noticed how the displacement of the subject from frame to frame was very small, depending on its relative speed with respect to the motion of the camera and its distance from the camera. This small displacement produced by objects moving at relatively low-medium speeds (walking person, moving bike or moving car) can be used as a motivation that the segmentation of neighbouring frames can be combined in order to obtain a more accurate segmentation of the present. In the next sections, this concept is regarded as the Image Buffer approach, figure 26 shows an illustration of an Image Buffer of size 2: it holds 2 frames from the past and merges them to the segmentation of the present frame.



Figure 18: Different types of annotations present in the Cityscapes dataset [6]. Upper figure shows an example of a densely annotated image (richer in detail). Bottom figure shows an example of a coarsely annotated image (lower level of detail). Image source: [4].

Apart from a straightforward combination of the pixel-classification output of neighbouring time frames (Image Buffer, section 5.1), a second approach that computes a weighted combination of the pixel-classification logits (section 4.1.4) produced by the baseline model will be introduced next.

As explained in section 4.1.4, the way in which DeepLab assigns the final classification labels to each pixel is by a previous calculation of a C -dimensional score array for each pixel, that together form a $H \times W \times C$ scoremap for the input image (C is the number of possible categories, 19 in the case of Cityscapes; H and W correspond to the height and width of the input image respectively). The C -dimensional array contains the likelihood of each pixel to belong to each one of the possible categories of the data set. The final pixel-labels are assigned by reducing the C -dimensional array of each pixel into one value that represents the index of the maximum value of the array, this is done by means of an argmax operation.

The weighted combination of the classification scores as an approximated version of a conditional probability (section 3.1) is the second approach that will be tested in the following sections. This method is referred as Attention Module (section 6).

4.2.1 Testing and evaluation

In order to stay truthful to the nominal conditions of baseline model, it would be necessary to test it using images with the same characteristics as the Cityscapes data set [6], this is 2048×1024 pixel images. However, it was not possible to find video sources with the same resolution as the Cityscapes data set and a 1920×1080 pixel resolution was adopted for the different tests. Although the difference on the number of total pixels between both formats is less than 2 percent, using lower resolution images than the ones used for training the weights of the baseline model might have an effect on the final segmentation. The study of this issue has not been covered and is added as one of the limitations in the discussions section (section 8).

The performance of both of the suggested approaches listed before, Image Buffer (5.1) and Attention Module (6) as well as the baseline performance (4.1.3) will be evaluated both quantitatively and qualitatively.

It is necessary to count with a groundtruth label annotation data set to quantitatively measure the segmentation performance. However, groundtruth annotations for multi-label semantic video segmentation are very costly and no available data sets that covers this need were found. The Densely Annotated Video Segmentation (DAVIS) 2016 benchmark [50] was chosen as an approximation for this requirement. It is formed by 50 densely annotated single-object short sequences, from which only 10 are suitable for the evaluation of this exercise (due to compatibility with the Cityscapes preset categories). The DAVIS categories that will be used for this study are:

- Breakdance-flare. A single person moving rapidly in the middle of the screen.

- Bus. A bus centered in the picture frame in a dynamic environment.
- Car-shadow. A car moving out from a shadow area.
- Car-turn. A car moving towards and outwards from the camera.
- Hike. A person moving slowly in the center of the frame.
- Lucia. A person moving slowly in the center of the frame.
- Rollerblade. A person moving fast from left to right of the frame.
- Swing. A person swinging back and forth and being temporarily occluded in the middle of the screen.
- Tennis. A person moving fast from right to left in the frame.

Since goal of this study is to improve the detection and the segmentation over time by reducing the number of missed classification and maintaining a consistent segmentation, the metrics used for the evaluation cover the temporal consistency and the accuracy.

A semantic image segmentation model that is consistent over time will produce a segmentation area with a smooth transition from frame to frame (depending on whether the tracked subject is moving or not). The segmentation area is calculated by counting the number of pixels classified with the target label at each time step. Afterwards, the frame-to-frame area variation is calculated as the difference of the area between consecutive frame pairs. A final computation of the standard deviation of these differences gives a global metric for the segmentation fluctuations (it is expected to obtain a lower number for more temporal consistent methods) that will be used for comparison of the different approaches.

The accuracy is calculated using the Intersection Over Union (described in section 4.1.3). And, in the same way as with the area, the frame-to-frame fluctuations of the accuracy are calculated as a comparison metric for all the approaches.

The qualitative evaluation consists on the observation and interpretation of the segmentation result of each one of the methods using different video sources.

The videos used for the qualitative evaluation are:

- Citadel - University of Twente
- Carré (modified) - University of Twente. One every ten frames was removed from the original clip to simulate a temporal occlusion or the faulty behavior of the camera sensor.
- Driving in a tunnel. Video source: [51].
- Driving under the rain. Video source: [52].
- Driving in the night. Video source: [53].
- Driving in low sun. Video source: [54]

4.2.2 Remarks

Videos are a very powerful source of information. In contrast with the analysis of pictures, videos provide objects with a temporal context as a series of frames that can be exploited to benefit segmentation. In order to do so, two different approaches will be evaluated: Image Buffer and Attention Module (section 4.2).

These two approaches will build up on top of DeepLabv3 [5] pre-trained on the Cityscapes data set [6], which is chosen as the baseline for this study due to its performance as the state-of-the-art semantic image segmentation model (section 4.1.3).

The results will be evaluated both qualitatively and quantitatively in a series of videos chosen to cover a wide variety of scenarios (section 4.2.1). The metrics used for the comparison of the different approaches are chosen to cover both the accuracy and the temporal consistency of the predictions (section 4.2.1).

The machine learning framework and programming language are fixed together: Python and Tensorflow. Python allows for rapid script prototyping and debugging and counts with lots of libraries that make working with images and arrays very natural. Tensorflow includes large amounts of documentation online, a very vivid community and it is being constantly updated with new utilities that offer new possibilities for the use of Deep Learning (section 4.1.2).

5 Design and implementation

This section covers in detail both of the suggested approaches used to provide temporal context to the semantic image segmentation: Image Buffer (section 5.1) and Attention Module (section 6).

5.1 Approach I: Image Buffer

Image Buffer is the first of the approaches studied to solve for the semantic image segmentation models' temporal inconsistency. It is the result of analyzing an object's location from frame-to-frame and the quality of the segmentation provided by DeepLabv3 (section 4.1.3) over consecutive frames.

The first premise follows from figure 21. *The translation of an object recorded at 30 fps over small batches of consecutive frames is negligible.*

The second premise follows from figure 26. *The combination of the segmentation in neighbouring frames helps completing the segmentation and avoiding temporal miss classifications.* In figure 26, 3 consecutive segmented frames were overlap in order to obtain an 'augmented segmentation'. The result of this experiment showed how the figure of a person was completed using the information of the 3 involved frames.

The origins of this fault in segmentation could be of different nature, from temporal physical occlusion such as flying objects covering the camera lens, to sensor saturation due to sun glare, or information loss due to system performance problems. The approach works as follows:

1. The present time frame is extracted from the video feed and passed through DeepLabv3 that computes the segmentation map.
2. The segmentation map is concatenated along with the segmentation of the 3 previous time frames contained in the Segmentation Buffer (figure 19).
3. The segmentation of the 4 evaluated frames is combined obtaining the augmented segmentation for the present time (figure 20).
4. Lastly, the Segmentation Buffer is updated by dropping the oldest frame and storing the last frame drawn from the original video.

To delimit this approach it is necessary to define the size of the segmentation buffer, this follows from the observation made in figure 21 that shows how the relative displacement on three consecutive frames is very small. For simplicity, the size of the image buffer is fixed to four: covers the present frame and three frames from the past.

This technique is only applied to a predefined subset of categories, the target categories. The reason for this discrimination is the concern towards the segmentation of the obstacles that can be found in the road. As a proof of concept, the target categories for the experiments are: 'person', 'rider', 'car' and 'bicycle'.

It is expected that this approach alleviates the defect of partially or completely missed classifications over the target categories. Nevertheless, the effect of this approach will only be apparent if the defect labels are missing for less than the size of the Image Buffer (if the labels are missing for longer than that, this approach is not able to recover them).

Overlapping past information for the inference of the present segmentation imposes a temporal lower bound to the object detection, at the same time, it reduces the time inconsistency alleviating the 'flickery' effect. Static elements or elements that move slowly with respect to the image frame are expected to benefit from this approach. The results of this application will be presented on the next section.

6 Approach II: Probabilistic Approach

Apart from a bare combination of the segmentation maps obtained at different time frames (section 5.1), there is also the possibility of making a more educated combination by modifying the probability map of each frame prior to the combination, resulting in an augmented segmentation. This approach is inspired by the transition probabilities in Markov Models that model the probability of an event transitioning between different possible states (section 3.1.2).

The intuition for this approach comes from the following line of thought: 'given that machine learning models are able to classify by calculating a confidence score (the logits) over a set of predefined labels, can those values be extended overtime (video inference) and used to influence the classification of consecutive frames?'. In other words, is it possible to establish a causal relation between past and present frame pixel-classification?



Figure 19: Block diagram of the Image Buffer approach (section 5.1). This block diagram depicts how the segmentation maps of 4 consecutive frames are combined into one (augmented segmentation).

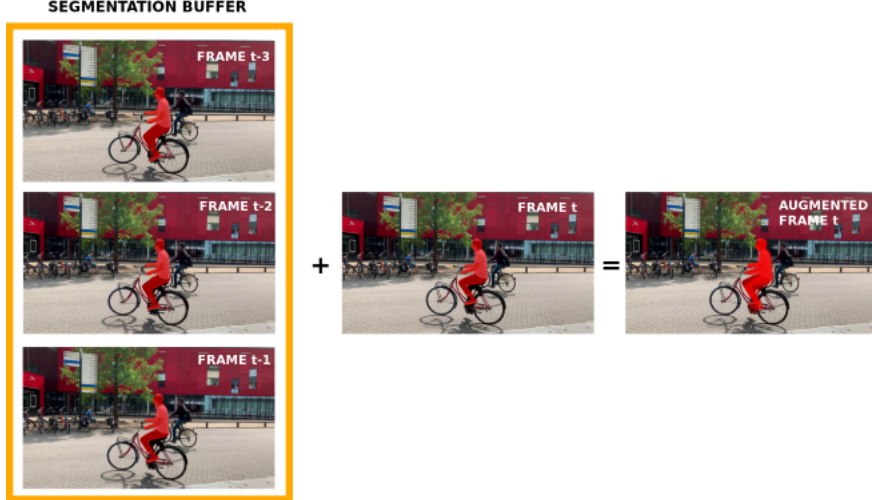


Figure 20: Conceptual representation of the Image-buffer approach. In this figure, the output is calculated as a combination of the segmentation in 3 consecutive past frames plus the segmentation of the present frame.

There are two problems that need to be addressed in order to create a temporal relation on the semantic image segmentation classification. First, the logit-map of each frame needs to be obtained and analyzed. Second, a relation between consecutive frames has to be defined.

6.1 Semantic image segmentation - Scoremap

In semantic segmentation, the logit-map is a $H \times W \times C$ matrix that contains, for each pixel in the image ($H \times W$) a vector of real numbers that represents the likelihood of belonging to each one of the predefined categories (C), the logits. The logit-map is located one step before the final assignation of labels (figure 22) and is formed by real numbers without any apparent bounds.

In order to establish a relation between consecutive frames, it is necessary to transform the logits of each pixel to a common scale for comparison. This can be done by means of a softmax function (equation 14) that transfer the raw prediction values of the neural network (the logits) into probabilities (logit-map into a probability-map).

$$S(C_i) = \frac{e^{C_i}}{\sum_j e^{C_j}} \quad (14)$$

where C_i refers to each element in the logits vector C .

Once that the probabilities have been determined, it is possible to establish a relation between consecutive frames.



Figure 21: This figure compares the translation of a moving object during 3 consecutive frames. Each of the two series shown in this figure (bike and truck) correspond to 3 consecutive frames extracted from two videos recorded at 30 fps. The upper series (from left to right) show a subject moving in a close plane horizontal to the camera. The lower series (from left to right) show a truck moving in a far plane horizontal to the camera. The further to the right image for both series is a mask overlap of each target over the 3 consecutive frames (zoomed in), it represents the relative displacement over time of these objects for a video recorded at 30 fps. It is observed how the relative displacement is minimal for both examples. The bike series, introduces how the combination of the history of an object with larger relative displacements may introduce a 'ghosting effect' to the resulting image. Apart from being dependent on the recording speed (fps) and distance to the camera, the relative displacement is also dependent on the relative speed between camera and object (although a speed figure comparison is not elaborated, this was observed along the different tests for this thesis study).

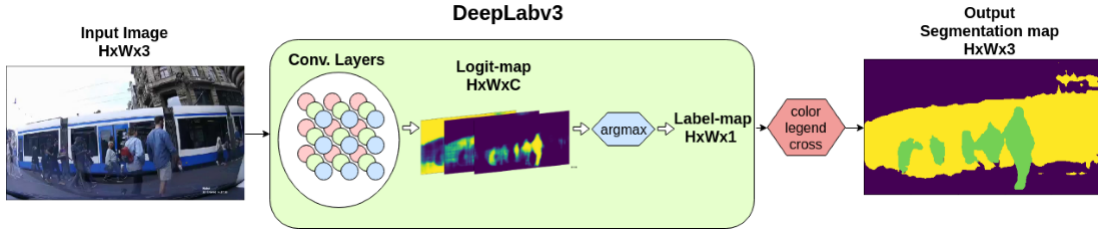


Figure 22: Graphical interpretation of the DeepLabv3 [5] semantic image segmentation tool-chain. The convolutional layers produce a $H \times W \times C$ matrix (the logit-map) that is reduced by means of an argmax function into a $H \times W \times 1$ matrix with the final labels of each pixel (the label-map). Finally an external function assigns a color value to each label.

6.2 Modeling videos as a weighted sum of frames

The Attention Module models the classification probability of the present as a weighted sum of consecutive frames (equation 15). The number of frames in consideration for the sum is four (three past frames plus the present frame), this is a conservative choice based on our observations on the test videos.

$$aug = I_0 \cdot p(t) + I_1 \cdot p(t-1) + I_2 \cdot p(t-2) + I_3 \cdot p(t-3) \quad (15)$$

aug is the resultant augmented logits (figure 23), I_n are the weights of frame $(t-n)$ and the probabilities $p(t-n)$ are extracted from the baseline segmentation model (section 4.1.4) after applying the transformation of the softmax function.

Weights estimation In theory, it should be possible to find the optimal weight values that shape equation 15 resulting in the probabilities with the smallest discrepancy with respect to the true segmentation. This is an optimization problem that requires the definition of a loss function and data-set with ground-truth annotations. In classification tasks the most common loss function is the cross-entropy function or the negative log likelihood[55] (equation 16)

$$L = - \sum_{c=1}^M y_{o,c} \log(p_{o,c}) \quad (16)$$

where M is the number of classes; $y_{o,c}$ is a binary indicator that the class label c is the correct classification for the observation o ; and $p_{o,c}$ is the predicted probability of observation o being of class c [56].

As opposed to the more common quadratic loss function, the cross-entropy loss function does not suffer slow learning due to the computation of small gradients [55]. The gradients computed on the cross-entropy loss function increase when the prediction moves further from the target value [55].

Besides the definition of a loss function, it is also necessary to count with a ground-truth annotation data-set. However, as mentioned in section 4.2.1, no public multi-label semantic video segmentation data-set was found and developing one was not feasible due to the lack of resources. As an alternative, in order to find the 'best' weight values, the equation 15 was tested using different parameter combinations on some of the videos listed in section 4.2.1. The value of the final weights can be found in table 3.

I_0	I_1	I_2	I_3	T
4	3	2	1	1

Table 3: Weight parameters for equation 15

As a result, using positive weights (bigger than 1) increases the sensitivity of the per-pixel classification, which added to the combination of successive frames result in a more consistent temporal segmentation (section 7.1). However, the increase in the sensitivity provokes a higher number of false positive classifications in the form of noise. The amount of false positive labels can be alleviated by setting up a threshold that pushes the augmented logits to zero if a minimum value is not reached (figure 23). Similar to the Image Buffer, this approach is only applied to a certain category targets as a proof that it can be used to leverage the classification of any category labels.

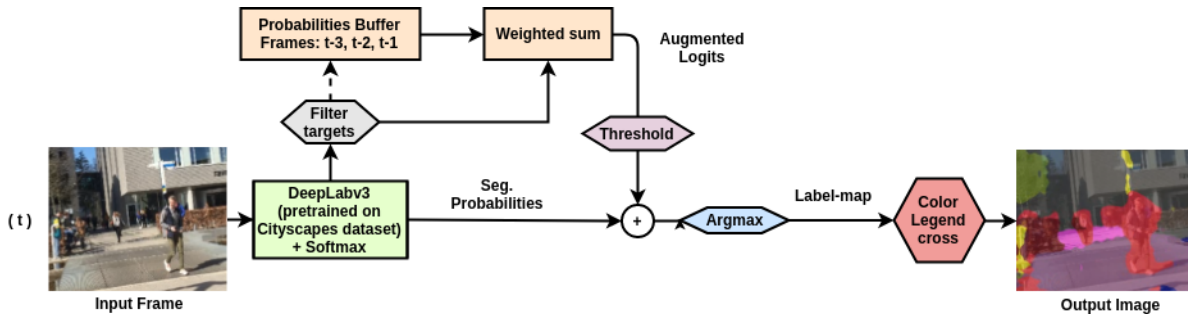


Figure 23: Block diagram of the Attention Module approach (section 6). This block diagram depicts how the classification probabilities of 4 consecutive frames are combined into one.

6.3 Experiments

The experiments are divided in two parts: a quantitative evaluation that measures the performance of each method using different metrics and a qualitative evaluation that is done by interpretation of the segmentation results.

7 Results

This section collects and analyzes the results for all the experiments listed in section 4.2.1. It also critically analyzes the followed methodology highlighting the best case scenarios and revealing the possible failure modes.

7.1 Quantitative results - Davis data-set

This section evaluates the performance of both suggested methods (Image Buffer and Attention Module), comparing them with the baseline segmentation (using DeepLabv3). Since the suggested methods are designed to *reduce the number of false negative by leveraging the temporal information encoded in image sequences-videos*, this section looks at the segmentation performance measuring and plotting the *Area overtime (AOT)* and *IOU overtime (IOU-OT)*. In addition, the frame to frame variation of both metrics will be calculated and plot side by side, expecting to find less variations on the approaches that handle past time information.

In order to quantify and compare the performance of each method, it is necessary to count with ground-truth annotations. However, it was not possible to find a data-set that covered this need and it was not feasible to create a custom one

given the time-line. For this reason, the DAVIS data-set [50] is used as an approximation with the limitation it can only evaluate one label at a time. The list of categories covered for this objective can be found in section 4.2.1.

Figures 24 and 25 give an example of the segmentation evaluation for the 'tennis' category of the DAVIS data-set [50]. Figure 24 shows an obvious result on how leveraging neighbouring frames benefits the final segmentation output. In this first figure in can be observed how the baseline segmentation is surpassed by both of the suggested methods, achieving a smoother shape with the Attention module approach. The main difference between both of the suggested methods is that the Image buffer directly uses the segmentation produced by the baseline model, while the Attention module by modifying the probability map of the segmentation is able to produce new segmentation labels that might benefit the final segmentation. In figure 24 it can also be observed how both of the suggested methods increase the number of false positive classifications, although it was intended to limit this number the study of its reduction is left as future work.

Figure 25 contains the graphs that measure the AOT, the IOU-OT and its variations for the 'tennis' category of the DAVIS data-set. The AOT is calculated to compare the differences in the production of labels of each method. As expected, it can be observed how the area detection for both of the suggested methods is superior than the baseline detection and the ground-truth annotations. The reason for this is the temporal combination and the increase in the production of false positive classifications. The IOU-OT indicates the accuracy of each method over time, expecting values closer to 1 for the best case scenarios. The results show how both the Image Buffer and the Attention Module generally reproduce a lower accuracy than the baseline method, which can be explained due to the increase of false positive classifications. Lastly, the variation of each metric is computed to asses the reliability of each method (a reliable application is expected to give consistent results overtime). For a perfect segmentation, the AOT variation should be similar to the ground-truth annotations and the IOU-OT variation equal to zero.

The dispersion of the variation of each metric is calculated by computing the standard deviation of the sequence; tables 4 and 5 gather these results. The variation is computed to measure the frame-to-frame consistency of the prediction, a segmentation that fully captures the dynamics of the sequence (that is consistent overtime) would result in a AOT Variation standard deviation equal to the ground-truth's one and a IOU-OT Variation standard deviation equal to zero.

	AOT Variation STD			
	Groundtruth	DeepLabv3 (Cityscapes)	Image Buffer	Attention Module
Breakdance-flare	2297873	4771063	3649613	3347300
Bus	1441019	4600729	3042283	2936702
Car-shadow	285037	1388070	1025686	1219912
Car-turn	1128675	1767648	1221533	1212808
Hike	342290	1992053	1044184	1268832
Lucia	443833	1430598	991134	1453644
Rollerblade	666624	3548873	3240213	2480139
Swing	1663433	4711279	4975625	4908373
Tennis	1073167	3690312	3523527	2904218

Table 4: AOT Variation STD for some of the DAVIS data-set [50] categories evaluated using different semantic segmentation approaches (section 4.2.1). Although the three approaches under study are far from achieving a Variation close to the groundtruth, the consistency of both the Image Buffer and the Attention Module outperforms the bare DeepLabv3 implementation.

Although the results shown in this section are a simplification (single-label classification) of what it might be present in a real driving scenario, these results can serve as a guideline on how the combination of frames affects to the final segmentation. Next section presents the results for a series of multi-label classification experiments.

7.2 Qualitative results - Video evaluation

In this subsection, the testing is extended to cover the multi-label detection. Due to the lack of groundtruth annotations, these experiments will be evaluated by the visual-quality of its results.

Figure 27 shows the segmentation performance of the baseline model (DeepLabv3) and its extension with the image buffer approach (detected area is contoured in red or blue) and the attention module approach. In particular, the extensions only leverage a set of predefined categories over the rest: **person, rider, bicycle, car and bus**. This is done as a proof of concept as well as due to hardware limitations, but it can be adapted to hold any other target categories.

	IOU-OT Variation STD (%)		
	DeepLabv3 (Cityscapes)	Image Buffer	Attention Module
Breakdance-flare	8.65	4.64	4.11
Bus	4.58	2.82	2.92
Car-shadow	2.97	1.75	1.81
Car-turn	1.53	0.93	0.89
Hike	4.68	1.57	1.49
Lucia	2.85	1.95	2.13
Rollerblade	14.67	7.25	5.89
Swing	5.56	3.69	3.78
Tennis	12.12	4.43	4.20

Table 5: IOU-OT Variation STD for some of the DAVIS data-set [50] categories evaluated using different semantic segmentation approaches (section 4.2.1). A robust segmentation would be translated in having a low STD, which means that the accuracy does not fluctuate over the sequence. It can be observed how the lowest values are obtained by the two approaches that exploit temporal information, the Image Buffer and the Attention Module.

7.2.1 Citadel - University of Twente

This video was taken on a normal day between lectures at the University of Twente. It was chosen to evaluate the performance of these methods in an environment rich on features with different targets present at the same time. Figure shows how both of the extensions help completing the partial segmentation of some targets.

Next section elaborates on the limitations of each method and makes a conclusion based on the results.

8 Discussion

The results show how the Image Buffer and Attention Module approaches can support the segmentation of a set of predefined target categories, this is due to the combination of information from neighbouring frames into the present segmentation.

Both of the extensions combine the segmentation of 3 past frames with the present frame. This is the result of the study performed and can only be applied to study-cases where the target object location does not differ considerably for 4 consecutive frames. In other words, it only applies to cases with a high recording-speed/target-relative-movement (w.r.t the camera) ratio. A low ratio will result on a 'ghosting effect' on the segmentation and a diffuse boundary definition of the targets.

The segmentation model also affects the final performance of both of the suggested extensions. Both of the extensions base their results on an initial baseline segmentation that is lastly modified. In the case of the Image Buffer this limitation is not very extreme and the final accuracy directly depend on the efficiency of the baseline model. In the other hand, the Attention Module modifies the probability-map of each frame by its multiplication with different weights (positive, greater than 1), this helps increasing the sensitivity of the detection of the target categories but in turn may produce false positive classifications.

Another limitation of the Attention Module approach is that its parameters were calculated heuristically, and the segmentation result might be sub-optimal. This was inevitable due to the lack of a sequential ground-truth data-set that could be used to find the optimal values of the weights and the threshold value (table 3).

The chosen data-set for training the baseline model also affects the final performance of the segmentation. It determines the final accuracy of the segmentation and sets some limitations on the resolution of the images and the covered scenarios. Cityscapes data-set, covers driving scenarios in urban areas which might be the reason why the baseline segmentation offers a low performance in figures, due to the angle of the camera. Besides that, Cityscapes gathered samples during spring and summer seasons, so it does not include adverse weather conditions nor poor illumination images.

Nevertheless, both of the extensions have proved how leveraging sequential information for the application of real-time predictions is beneficial for the consistency of the results. When applied to autonomous navigation, creating an image segmentation training data-set that covers all the possible scenarios is very difficult and holding the information of past frames adds a protection layer against failure modes.

9 Conclusions

The evaluation of the baseline performance, showed that the output segmentation over a sequence is irregular. This is a problem when the application relies on the frame segmentation as a main source of information. In order to attenuate these variations, both of the extension approaches (Image Buffer and Attention Module) combine the information of neighbouring frames to make a more educated segmentation of the present. Tables 4 and 5 show the effect of these extensions would successfully reduce the fluctuations on the segmentation overtime.

This study also showed some cases in which the baseline model was not able to detect a target in the field of view. Our new frameworks proved to reduce the number of false negative classifications. The Image Buffer approach sets a time lower bound on the segmentation providing a safety margin over sudden faulty modes. The Attention Module, due to the modifications on the probability map, is able to increase the sensitivity of the detection of a set of predefined targets while at the same time providing the advantages of the Image Buffer approach. Which can be very useful for the detection of obstacles in the case of autonomous navigation.

Both of the extensions (Image Buffer and Attention Module) require to store an array of dimensions: $M \times H \times W \times N$. Where M is the number of target categories, H and W the dimensions of the image source and N the number of frames to be combined. This can be computationally very costly to be evaluated in a real-time implementation and requires a well selected hardware framework.

We can also suggest to use this methodology during the training phase of the segmentation model. The final user can create artificial annotations for the categories that appear to be more challenging for the baseline model and use them as ground-truth annotations for further training. This would expect to improve the segmentation over those target categories and get rid of the computational constraint imposed by having to store an array for the segmentation augmentation.

As a future work, we believe that different ways using the suggested frameworks could be studied. Instead of overlapping the segmentation results of the baseline model or making a weight sum relation between consecutive frames, a more elaborated relation that uses probabilistic relations can be defined.

The combination of sequential information and enhancement of the probability-map results in an increase of false positive classifications in the form of segmentation noise. There are different ways that can help alleviate this problem, while at the same time raising the overall accuracy of the segmentation. Some of them are:

- Fine tuning the parameters that define the Attention Module. In such a way that, the values that do not reach a minimum after the probability augmentation are pushed to 0 and therefore will not be assigned the target label.
- Using different temporal modules with different sensitivity values. After the computation of the augmented probabilities, the results will be compared and only the classifications with the highest agreement will be output.
- Limiting the work-space of the temporal modules. The augmented segmentation can be applied only to a certain region of interest, such as just the driving-space. This can alleviate the production of false positive classifications and increase the performance of the algorithm.
- Combining this method with a 3D map estimation. After the calculation of the augmented segmentation map, it could be projected onto a 3D map of the environment, assigning labels to the 3D objects and discarding the labels that do not project into any plane (or very far away).

Another extension of this study could be to instead of basing the augmentation on only past frames, an estimated prediction of nearby future states ($t+1$, $t+2$...) could be calculated and added into the combination. At the same time, given a sequential fully annotated data-set could provide the optimal set of parameters that define the relations between adjacent frames.

On top of that, these extensions could be applied to create an artificial sequential data-set. Using the results of the baseline model with the extension on the temporal domain could be used to generate short annotated sequences. These sequences can then be used to train deep learning architectures that embed the temporal behavior on its structure. Deep learning models such as convLSTM [57], GRFP [13] or the Multiclass semantic video segmentation [15] can be live-trained with these temporal extensions, creating a self-supervised segmentation pipeline.

It could be interesting to study the performance of semantic image segmentation models and its temporal extension from the inference-speed point of view. Although this study was performed on the state-of-the-art semantic image segmentation model (highest in accuracy), other models designed to perform at much higher speed rates can influence the type of solution needed for the temporal analysis.

Finally, finding new applications where this method can be applied. One of the highlights of this study is that slow environments benefit from sequential information, helping to smooth and to complete partial segmentation results (figure 27). Of course, applications with different types of sequential data can also be analyzed under the same suggested approaches. This indicates the potential impact of our new sequential frameworks in a large field of video and image analysis.

References

- [1] Dyfed Loesche. How americans commute to work. 2017. <https://www.statista.com/chart/11355/how-americans-commute-to-work/>.
- [2] Niall McCarthy. Fewer americans are driving to work. 2018. <https://www.statista.com/chart/15398/the-share-of-us-workers-aged-18--who-commute-to-work-using-the-following-means/>.
- [3] Yann LeCun, Patrick Haffner, Léon Bottou, and Yoshua Bengio. Object recognition with gradient-based learning. In *Shape, Contour and Grouping in Computer Vision*, 1999.
- [4] Cityscapes-Team. Cityscapes dataset. 2019. <https://www.cityscapes-dataset.com/>.
- [5] Liang-Chieh Chen, George Papandreou, Florian Schroff, and Hartwig Adam. Rethinking atrous convolution for semantic image segmentation. *ArXiv*, abs/1706.05587, 2017.
- [6] Marius Cordts, Mohamed Omran, Sebastian Ramos, Timo Rehfeld, Markus Enzweiler, Rodrigo Benenson, Uwe Franke, Stefan Roth, and Bernt Schiele. The cityscapes dataset for semantic urban scene understanding. In *Proc. of the IEEE Conference on Computer Vision and Pattern Recognition (CVPR)*, 2016.
- [7] Kevin P. Murphy. Machine learning - a probabilistic perspective. In *Adaptive computation and machine learning series*, 2012.
- [8] Andrew Y. Ng and Michael I. Jordan. On discriminative vs. generative classifiers: A comparison of logistic regression and naive bayes. In *NIPS*, 2001.
- [9] Julia Lasserre, Christopher M. Bishop, José M. Bernardo, M. Jesús Bayarri, James O. Berger, A. Philip Dawid, David Heckerman, Arlette Miller Smith, and M. A. West. Generative or discriminative? getting the best of both worlds. 2007.
- [10] Pedro M. Domingos and Michael J. Pazzani. Beyond independence: Conditions for the optimality of the simple bayesian classifier. In *ICML*, 1996.
- [11] Victor Powell. Markov chains, 2014. <http://setosa.io/ev/markov-chains/>.
- [12] D. Conklin. Music generation from statistical models. In *AISB Symposium on Artificial Intelligence and Creativity in the Arts and Sciences*, pages 30–35, 2003.
- [13] David Nilsson and Cristian Sminchisescu. Semantic video segmentation by gated recurrent flow propagation. *2018 IEEE/CVF Conference on Computer Vision and Pattern Recognition*, pages 6819–6828, 2016.
- [14] Abhijit Kundu, Vibhav Vineet, and Vladlen Koltun. Feature space optimization for semantic video segmentation. *2016 IEEE Conference on Computer Vision and Pattern Recognition (CVPR)*, pages 3168–3175, 2016.
- [15] Buyu Liu and Xuming He. Multiclass semantic video segmentation with object-level active inference. *2015 IEEE Conference on Computer Vision and Pattern Recognition (CVPR)*, pages 4286–4294, 2015.
- [16] Ondrej Miksik, Daniel Munoz, J. Andrew Bagnell, and Martial Hebert. Efficient temporal consistency for streaming video scene analysis. *2013 IEEE International Conference on Robotics and Automation*, pages 133–139, 2013.
- [17] Nicolai Wojke, Alex Bewley, and Dietrich Paulus. Simple online and realtime tracking with a deep association metric. *2017 IEEE International Conference on Image Processing (ICIP)*, pages 3645–3649, 2017.
- [18] Alex Bewley, ZongYuan Ge, Lionel Ott, Fabio Tozeto Ramos, and Ben Upcroft. Simple online and realtime tracking. *2016 IEEE International Conference on Image Processing (ICIP)*, pages 3464–3468, 2016.
- [19] Ronny Restrepo. What is semantic segmentation? 2017. http://ronny.rest/tutorials/module/seg_01/segmentation_01_intro/.
- [20] Hengshuang Zhao, Xiaojuan Qi, Xiaoyong Shen, Jianping Shi, and Jiaya Jia. Icnet for real-time semantic segmentation on high-resolution images. *ArXiv*, abs/1704.08545, 2017.
- [21] Liang-Chieh Chen, George Papandreou, Iasonas Kokkinos, Kevin Murphy, and Alan L. Yuille. Deeplab: Semantic image segmentation with deep convolutional nets, atrous convolution, and fully connected crfs. *IEEE Transactions on Pattern Analysis and Machine Intelligence*, 40:834–848, 2016.

- [22] Xiaoxiao Li, Ziwei Liu, Ping Luo, Chen Change Loy, and Xiaoou Tang. Not all pixels are equal: Difficulty-aware semantic segmentation via deep layer cascade. *2017 IEEE Conference on Computer Vision and Pattern Recognition (CVPR)*, pages 6459–6468, 2017.
- [23] Heng Fan, Xue Mei, Danil V. Prokhorov, and Haibin Ling. Multi-level contextual rnns with attention model for scene labeling. *IEEE Transactions on Intelligent Transportation Systems*, 19:3475–3485, 2016.
- [24] Guosheng Lin, Chunhua Shen, Ian D. Reid, and Anton van den Hengel. Efficient piecewise training of deep structured models for semantic segmentation. *2016 IEEE Conference on Computer Vision and Pattern Recognition (CVPR)*, pages 3194–3203, 2015.
- [25] Tobias Pohlen, Alexander Hermans, Markus Mathias, and Bastian Leibe. Full-resolution residual networks for semantic segmentation in street scenes. *2017 IEEE Conference on Computer Vision and Pattern Recognition (CVPR)*, pages 3309–3318, 2016.
- [26] Golnaz Ghiasi and Charless C. Fowlkes. Laplacian pyramid reconstruction and refinement for semantic segmentation. In *ECCV*, 2016.
- [27] Guosheng Lin, Anton Milan, Chunhua Shen, and Ian D. Reid. Refinenet : Multipath refinement networks with identity mappings for high-resolution semantic segmentation. 2016.
- [28] Xin Li, Zequn Jie, Wei Wang, Changsong Liu, Jimei Yang, Xiaohui Shen, Zhe L. Lin, Qiang Chen, Shuicheng Yan, and Jiashi Feng. Foveanet: Perspective-aware urban scene parsing. *2017 IEEE International Conference on Computer Vision (ICCV)*, pages 784–792, 2017.
- [29] Josip Krapac, Ivan Kreso, and Sinisa Segvic. Ladder-style densenets for semantic segmentation of large natural images. *2017 IEEE International Conference on Computer Vision Workshops (ICCVW)*, pages 238–245, 2017.
- [30] Xiaojie Jin, Xin Li, Huaxin Xiao, Xiaohui Shen, Zhe L. Lin, Jimei Yang, Yunpeng Chen, Jian Dong, Luoqi Liu, Zequn Jie, Jiashi Feng, and Shuicheng Yan. Video scene parsing with predictive feature learning. *2017 IEEE International Conference on Computer Vision (ICCV)*, pages 5581–5589, 2016.
- [31] Rui Zhang, Sheng Tang, Min Lin, Jintao Li, and Shuicheng Yan. Global-residual and local-boundary refinement networks for rectifying scene parsing predictions. In *IJCAI*, 2017.
- [32] Rui Zhang, Sheng Tang, Yongdong Zhang, Jintao Li, and Shuicheng Yan. Scale-adaptive convolutions for scene parsing. *2017 IEEE International Conference on Computer Vision (ICCV)*, pages 2050–2058, 2017.
- [33] Falong Shen, Rui Gan, Shuicheng Yan, and Gang Zeng. Semantic segmentation via structured patch prediction, context crf and guidance crf. *2017 IEEE Conference on Computer Vision and Pattern Recognition (CVPR)*, pages 5178–5186, 2017.
- [34] Panqu Wang, Pengfei Chen, Ye Yuan, Ding Liu, Zehua Huang, Xiaodi Hou, and Garrison W. Cottrell. Understanding convolution for semantic segmentation. *2018 IEEE Winter Conference on Applications of Computer Vision (WACV)*, pages 1451–1460, 2017.
- [35] Raghudeep Gadde, Varun Jampani, and Peter V. Gehler. Semantic video cnns through representation warping. *2017 IEEE International Conference on Computer Vision (ICCV)*, pages 4463–4472, 2017.
- [36] Zifeng Wu, Chunhua Shen, and Anton van den Hengel. Wider or deeper: Revisiting the resnet model for visual recognition. *ArXiv*, abs/1611.10080, 2016.
- [37] Hengshuang Zhao, Jianping Shi, Xiaojuan Qi, Xiaogang Wang, and Jiaya Jia. Pyramid scene parsing network. *2017 IEEE Conference on Computer Vision and Pattern Recognition (CVPR)*, pages 6230–6239, 2016.
- [38] Liang-Chieh Chen, George Papandreou, Iasonas Kokkinos, Kevin Murphy, and Alan L. Yuille. Semantic image segmentation with deep convolutional nets and fully connected crfs. *CoRR*, abs/1412.7062, 2014.
- [39] Evan Shelhamer, Jonathan Long, and Trevor Darrell. Fully convolutional networks for semantic segmentation. *2015 IEEE Conference on Computer Vision and Pattern Recognition (CVPR)*, pages 3431–3440, 2014.
- [40] Mark Everingham, Luc Van Gool, Christopher K. I. Williams, John M. Winn, and Andrew Zisserman. The pascal visual object classes (voc) challenge. *International Journal of Computer Vision*, 88:303–338, 2009.
- [41] Dominik Scherer, Andreas C. Müller, and Seven Behnke. Evaluation of pooling operations in convolutional architectures for object recognition. In *ICANN*, 2010.
- [42] Fisher Yu and Vladlen Koltun. Multi-scale context aggregation by dilated convolutions. *CoRR*, abs/1511.07122, 2015.
- [43] Kristen Grauman and Trevor Darrell. The pyramid match kernel: discriminative classification with sets of image features. *Tenth IEEE International Conference on Computer Vision (ICCV’05) Volume 1*, 2:1458–1465 Vol. 2, 2005.

- [44] Svetlana Lazebnik, Cordelia Schmid, and Jean Ponce. Beyond bags of features: Spatial pyramid matching for recognizing natural scene categories. *2006 IEEE Computer Society Conference on Computer Vision and Pattern Recognition (CVPR'06)*, 2:2169–2178, 2006.
- [45] Isma Hadji and Richard Wildes. What do we understand about convolutional networks? 03 2018.
- [46] Kaiming He, Xiangyu Zhang, Shaoqing Ren, and Jian Sun. Deep residual learning for image recognition. *2016 IEEE Conference on Computer Vision and Pattern Recognition (CVPR)*, pages 770–778, 2015.
- [47] Gabriel J. Brostow, Jamie Shotton, Julien Fauqueur, and Roberto Cipolla. Segmentation and recognition using structure from motion point clouds. In *ECCV (1)*, pages 44–57, 2008.
- [48] Timo Scharwächter. Daimler urban segmentation. <http://www.6d-vision.com/scene-labeling>.
- [49] Andreas Geiger, Philip Lenz, Christoph Stiller, and Raquel Urtasun. Vision meets robotics: The kitti dataset. *International Journal of Robotics Research (IJRR)*, 2013.
- [50] F. Perazzi, J. Pont-Tuset, B. McWilliams, L. Van Gool, M. Gross, and A. Sorkine-Hornung. A benchmark dataset and evaluation methodology for video object segmentation. In *Computer Vision and Pattern Recognition*, 2016.
- [51] Kroonenberg. A drive downtown amsterdam. 2019. <https://www.youtube.com/watch?v=JXJ-YiNeKKI>.
- [52] TexasHighDef. A drive downtown amsterdam. 2018. <https://www.youtube.com/watch?v=mjtVs2E4zPg>.
- [53] Dash Cam Tours. Night driving on california freeway. no music. 2017. <https://www.youtube.com/watch?v=ICGTcCinouI>.
- [54] konradc12. Driving in low sun. 2018. <https://www.youtube.com/watch?v=kOor2-vQ3VE>.
- [55] Michael Nielsen. Neural networks and deep learning. 2019. http://neuralnetworksanddeeplearning.com/chap3.html#the_cross-entropy_cost_function.
- [56] ML-cheatsheet. Loss functions. 2018. https://ml-cheatsheet.readthedocs.io/en/latest/loss_functions.html#cross-entropy.
- [57] Xingjian Shi, Zhoung Chen, Hao Wang, Dit-Yan Yeung, Wai-Kin Wong, and Wang chun Woo. Convolutional lstm network: A machine learning approach for precipitation nowcasting. *ArXiv*, abs/1506.04214, 2015.

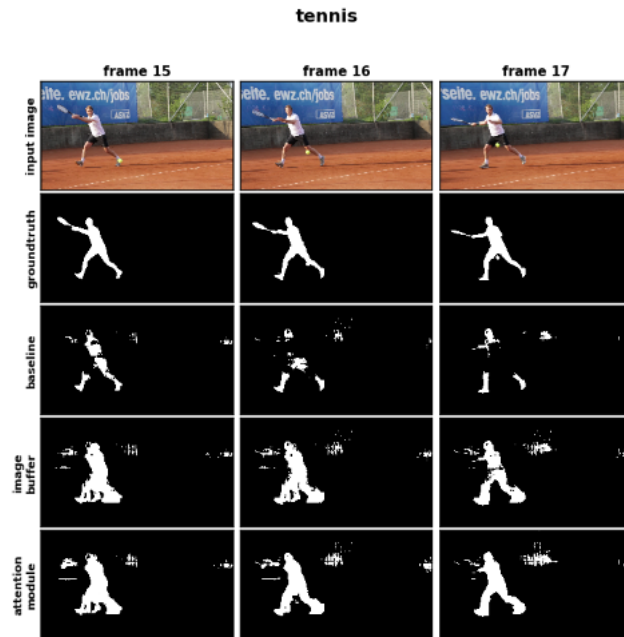


Figure 24: Figure comparison of the segmentation of 3 consecutive frames and its corresponding groundtruth annotation. It can be observed how both the Image Buffer and the Attention Module achieve a better segmentation of the 'person' category although there is also an increase in the amount of false positive classifications. Sequence source: DAVIS dataset [50] - 'tennis' category.

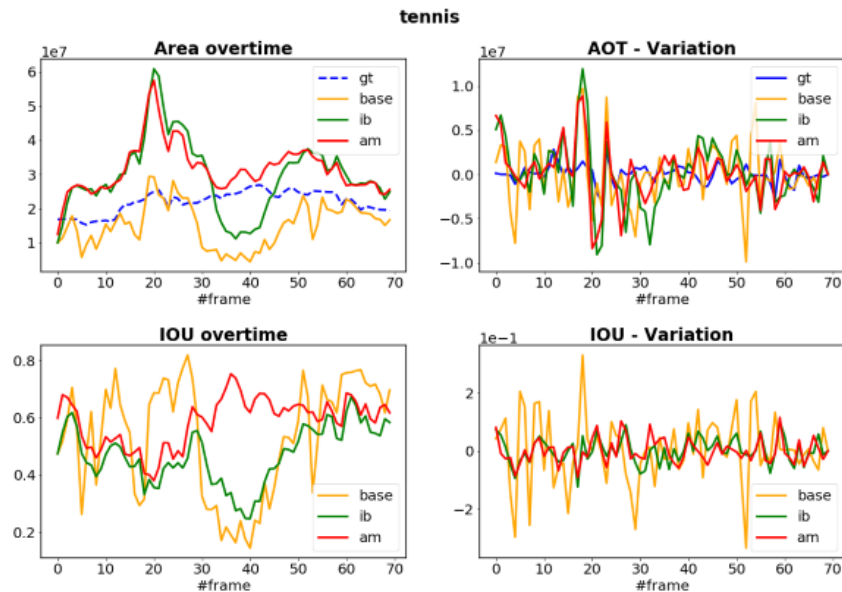


Figure 25: Graph evaluation of the 'tennis' category (DAVIS dataset [50]) using the metrics defined in section 4.2.1. The upper graphs shows how the AOT of both suggested approaches is higher than the baseline model, although they tend to have a lower variation. The lower graphs show how both of the suggested approaches tend to be less accurate than the baseline segmentation, this can be reasoned by the increased production of false positive classifications. In addition, the IOU variation for both the IB and AT is lower than for the baseline.

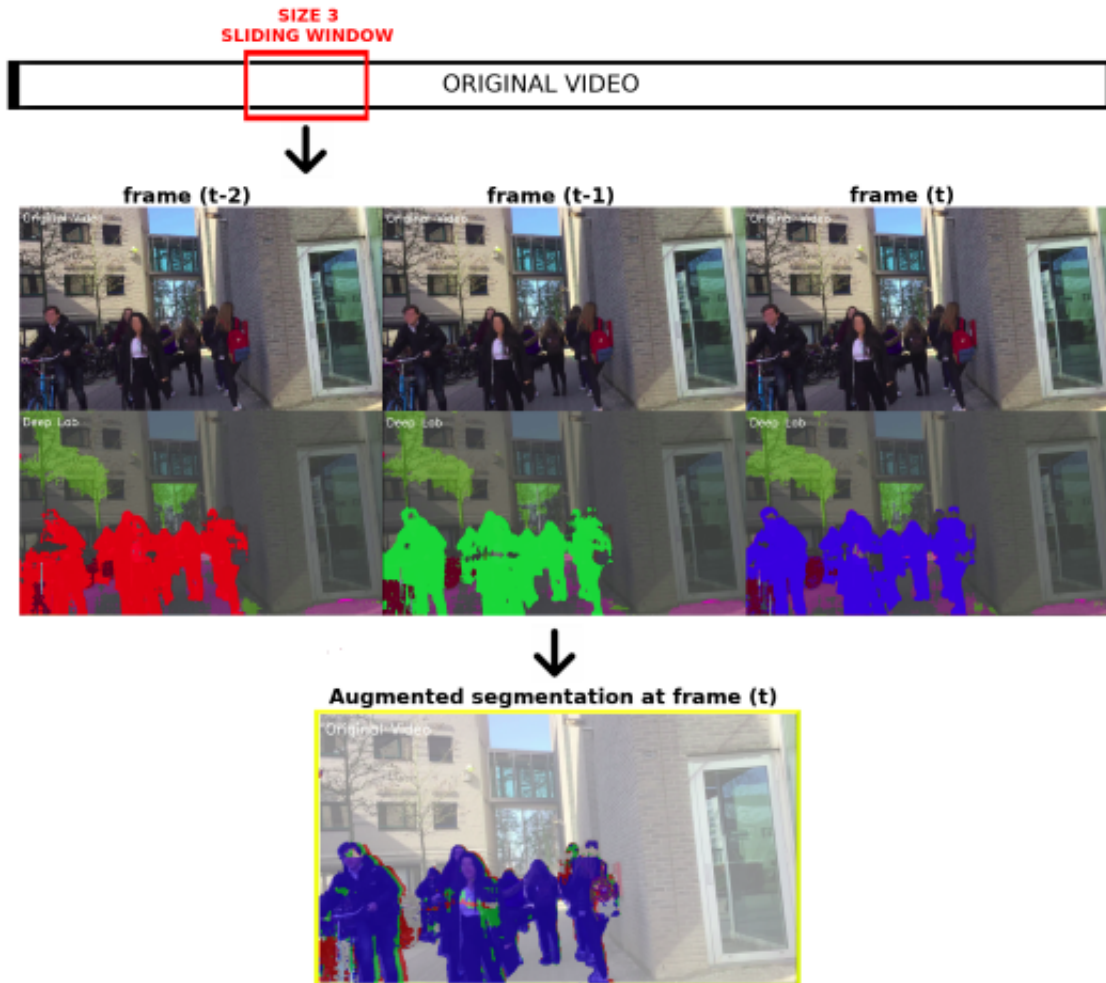


Figure 26: Conceptual figure that shows how the combination of the segmentation of a particular target (person in this case) of neighbouring frames can be beneficial for the segmentation at the present time. From top to bottom: 3 consecutive frames are extracted from the original video using a sliding window that covers the present frame and 2 other consecutive frames in the past (the extraction can be done for more than 3 frames); the baseline segmentation model (DeepLabv3 on Cityscapes) is applied to each one of these frames, the person label is highlighted in a different color (red, green, blue) for each frame in order to improve the visualization; the hypothetical augmented segmentation output is constructed by overlapping the segmentation of the 3 consecutive frames in the sliding window (bottom figure). It can be observed how the Augmented segmentation at frame (t) contains parts of the segmentation of each of the examined frames. The results show how the wholes in the segmentation of the man in the left and the woman in the middle at time (t) are 'filled' by the segmentation of frames at times (t-2) and (t-1).

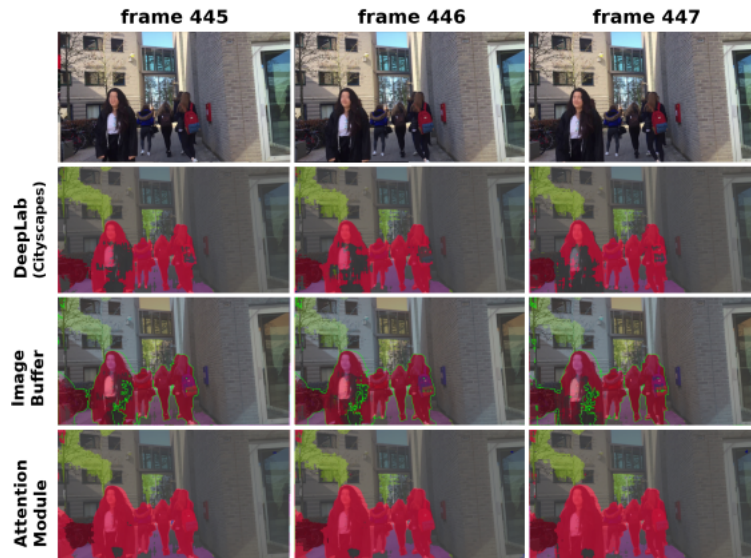


Figure 27: Figure comparison of the segmentation of three consecutive frames for a video sequence recorded outdoors in the presence of multiple target categories. It can be observed how the baseline segmentation (DeepLab) is able to detect most of the subjects and how the suggested extensions help completing the segmentation.